JACS
JOURNAL OF THE AMERICAN CHEMICAL SOCIETY
Communication
pubs.acs.org/JACS

Ultraviolet Spectrum and Photochemistry of the Simplest Criegee Intermediate CH_2OO

Joseph M. Beames, Fang Liu, Lu Lu, and Marsha I. Lester*

Department of Chemistry, University of Pennsylvania, Philadelphia, Pennsylvania 19104-6323, United States

ABSTRACT: Ozonolysis of alkenes in the troposphere produces Criegee intermediates, which have eluded detection in the gas phase until very recently. This laboratory has synthesized the simplest Criegee intermediate within a quartz capillary tube affixed to a pulsed valve to cool and isolate CH_2OO in a supersonic expansion. UV excitation resonant with the B $^1A' \leftarrow$ X $^1A'$ transition depletes the ground-state population of CH_2OO, which is detected by single-photon ionization at 118 nm. The large UV-induced depletion (approaching 100%) near the peak of the profile at 335 nm is indicative of rapid dissociation, consistent with the repulsive B $^1A'$ potential along the O−O coordinate computed theoretically. The experimental spectrum is in very good accord with the absorption spectrum calculated using the one-dimensional reflection principle. The B ← X spectrum is combined with the solar actinic flux to estimate an atmospheric lifetime for CH_2OO at midday on the order of ∼1 s with respect to photodissociation.

Alkenes are important volatile organic compounds in the Earth's troposphere. Ethene and propene are primarily produced by motor vehicles, while others originate from anthropogenic and biogenic sources, including isoprene and terpenes emitted by plants and trees. Alkenes are oxidized in the atmosphere through direct gas-phase reaction with ozone (O_3) as well as through OH and NO_3 radical-initiated processes.[1−3] Ozonolysis plays a major role in the tropospheric removal of these unsaturated hydrocarbons, contributing significantly to both their day- and nighttime chemistry. Additionally, these reactions provide a nonphotolytic source of OH radicals,[4−6] which may elevate atmospheric OH concentrations.

Ozonolysis of alkenes occurs through ozone addition across the double bond, producing a primary ozonide, followed by rapid rearrangement and dissociation to generate a carbonyl oxide, known as the Criegee biradical intermediate, and an aldehyde (or ketone) product.[7−9] The Criegee intermediates are formed with large excess internal energy and can undergo subsequent reactions, such as unimolecular decomposition and isomerization, or alternatively lose the excess energy through stabilizing collisions. Subsequent decay processes of energized Criegee intermediates yield OH radicals and other products of atmospheric significance, including HO_2, CO, CO_2, CH_3, and H_2CO. In addition, Criegee intermediates undergo further reactions with tropospheric trace constituents, as indicated in recent field measurements,[10] to produce secondary organic aerosols and phytotoxic species.

Although Criegee intermediates have been inferred in ozonolysis reactions for decades,[7] the first direct detection of the simplest Criegee intermediate, CH_2OO, in the gas phase was only recently reported.[11] In 2012, Taatjes and co-workers demonstrated a new synthetic method for generating CH_2OO in a flow cell at low pressures:[12,13]

$$CH_2I_2 + 248\ \text{nm light} \rightarrow CH_2I + I$$

$$CH_2I + O_2 \rightarrow CH_2OO + I$$

In the atmosphere, this Criegee intermediate would be generated from ozonolysis of ethene. Welz et al.[12] showed that remarkable information can be obtained by using tunable vacuum ultraviolet (VUV) radiation from a synchrotron source to establish the photoionization threshold for CH_2OO (10.02 eV), which can be readily distinguished from more stable isomers with the same mass (m/z 46) but higher photoionization thresholds (dioxirane at 10.82 eV and formic acid at 11.33 eV); the more stable isomers were not observed with this synthetic approach. They then utilized fixed VUV ionization (10.5 eV) with mass spectrometric detection to probe directly the Criegee intermediate and its rate of reaction with trace tropospheric constituents.[12,14] In particular, they demonstrated that the bimolecular reactions of CH_2OO with SO_2 and NO_2 are far more rapid than previously thought, which may substantially change predictions of tropospheric aerosol formation.

This new synthetic route was implemented in the present study to generate CH_2OO, but the low pressure flow cell was replaced with a quartz capillary tube affixed to a pulsed valve as the reaction vessel. (This approach mirrors the one employed in this laboratory in previous studies of the HOONO isomer of $HONO_2$.[15]) CH_2I_2 vapor was entrained in a 20% O_2/Ar carrier gas mixture at 25 psi and photolyzed with 248 nm radiation from an excimer laser as the gas pulse passed through the capillary tube (1 mm bore, 26 mm length). The photoproducts (and unreacted gases) then were cooled in a supersonic expansion and flowed downstream as isolated species (∼100 μs flight time) to a time-of-flight mass spectrometer, where they were ionized with a single photon of VUV radiation at 118 nm (10.5 eV; generated by frequency tripling of the third harmonic output of a Nd:YAG laser in a Xe:Ar gas cell). We observed a signal at m/z 46 when 248 nm photolysis occurred along the capillary; no m/z 46 signal was observed when photolysis occurred downstream of the capillary exit or the photolysis laser was blocked. Only the Criegee intermediate and no other CH_2OO isomers can be photoionized at 10.5 eV.[12]

Received: October 27, 2012
Published: December 3, 2012

   dx.doi.org/10.1021/ja310603j | J. Am. Chem. Soc. 2012, 134, 20045−20048

Spectroscopic studies of the Criegee intermediate were carried out by electronic excitation of the B $^1A' \leftarrow X\ ^1A'$ transition of CH_2OO using tunable UV laser radiation (280–420 nm). The UV radiation was generated by frequency doubling of the output of a Nd:YAG-pumped dye laser utilizing many dyes (i.e., Rh 590, 610, and 640; DCM; LDS 698, 750, 751, 765, and 821; and dye mixtures) and calibrated with a wavemeter. The experimental approach is illustrated schematically in Figure 1. UV excitation resonant with the B ← X transition depletes the ground-state population of CH_2OO, which is detected after a short time delay (Δt = 100 ns) with the VUV photoionization laser as a reduced signal at m/z 46.

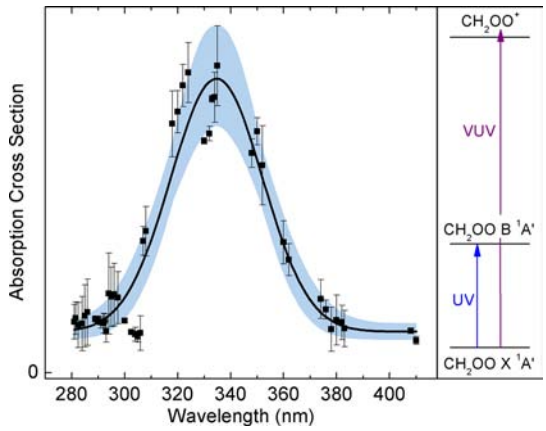

Figure 1. Experimental UV spectrum of CH_2OO isolated in a pulsed supersonic expansion. The absorption cross section was derived from the UV-induced depletion of the ground state and the corresponding VUV photoionization signal at m/z 46. The smooth curve is a fit to a simple Gaussian form; the uncertainty is illustrated by the blue-shaded region.

Significant depletion of the CH_2OO photoionization signal was observed upon UV excitation in the 320–350 nm spectral region. The UV energy was set at ~1 mJ/pulse throughout this central region of the spectrum and yielded depletions on the order of 60% in magnitude. Substantially larger UV-induced depletion (approaching 100%) was readily achieved with an energy of ~2.5 mJ/pulse at 320 nm. By contrast, the large frequency-doubled outputs available from Rh dyes (up to 5 mJ/pulse) at shorter wavelengths yielded smaller absolute depletions from 310 to 280 nm. Similarly, smaller depletions were observed at longer wavelengths (beyond 360 nm with up to 2 mJ/pulse) in the central region.

The absorption cross section $\sigma(\lambda)$ for CH_2OO, which was obtained from the magnitude of the depletion of the ground state $(N_0 - N)/N_0$ (with abundances N_0 before and N after UV irradiation) and the photon flux $\Phi(\lambda)$ using the expression

$$\sigma(\lambda) = -\ln(N/N_0)/\Phi(\lambda)$$

is plotted in Figure 1. The UV-induced depletion was measured at wavelengths near the maximum (within 10%) of each doubled dye curve with error bars determined from repeated measurements. The absorption spectrum was fit to a simple Gaussian plus offset form to guide the eye and extract the peak at 335 nm and the breadth of 40 nm (fwhm). The absolute absorption cross section was estimated to be $\sigma \approx 5 \times 10^{-17}$ cm^2 molecule^{-1} at the peak of the spectrum, indicating very strong UV absorption by the Criegee intermediate. The large magnitude of the depletion also demonstrates that CH_2OO promoted to the excited B $^1A'$ electronic state undergoes rapid dynamics, affording depletions significantly greater than 50%.

Complementary electronic structure calculations were undertaken to map the singlet potential energy surfaces of CH_2OO for the ground X $^1A'$ and excited B $^1A'$ electronic states along the O–O radial coordinate (Figure 2). The potentials were obtained using CASSCF(18,14) with an AVTZ basis set as implemented in the Molpro computational suite.[16] Prior theoretical calculations (CASSCF and CASPT2) predicted a strong B ← X transition at ~4 eV (310 nm) with large oscillator strength (f = 0.1),[17] while very recent calculations (EOM-CCSD/AVQZ//QCISD/AVTZ) yielded a vertical excitation energy of 3.9 ± 0.1 eV (318 ± 8 nm) and f = 0.15.[18] These correspond to peak absorption cross sections of (2–3) × 10^{-17} cm^2 molecule^{-1}. The present calculations and those in ref 17 indicate that the excited B $^1A'$ potential is fully repulsive along the O–O coordinate. As a result, CH_2OO promoted to the B $^1A'$ state undergoes direct dissociation, yielding formaldehyde and excited O(^{1}D) products at the lowest asymptotic limit:

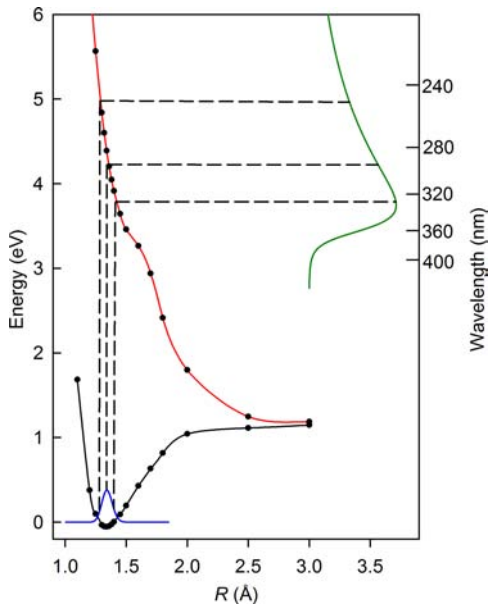

Figure 2. Prediction of the UV absorption spectrum of CH_2OO (green) by the reflection principle using the X $^1A'$ (black) and B $^1A'$ (red) potential curves along the radial O–O coordinate R obtained from CASSCF calculations (points).

$$CH_2OO(B\ ^1A') \rightarrow H_2CO(X\ ^1A_1) + O(^1D)$$

In addition, nonadiabatic coupling may enable CH_2OO B $^1A'$ to dissociate via an excited singlet surface to H_2CO(a $^3A_1$) and ground O(^{3}P) products. Similar photochemistry occurs for isoelectronic O_3 in the analogous Hartley band,[19] where avoided crossings between excited electronic states lead to O(^{3}P) and O(^{1}D) products.[20]

The repulsive nature of the CH_2OO B $^1A'$ potential surface makes it straightforward to predict the B ← X absorption spectrum using the classical one-dimensional reflection principle,[21] as shown previously for O_3.[22] The absorption spectrum is derived from the projection of the ground-state coordinate distribution for a harmonic oscillator onto the gradient of the B $^1A'$ excited-state potential (V) along the O–O radial coordinate (R). This yields the absorption cross section σ

dx.doi.org/10.1021/ja310603j | J. Am. Chem. Soc. 2012, 134, 20045–20048

as a function of energy E in the excited state, subject to the approximations detailed in ref 21:

$$\sigma(E) \approx e^{-\mu\omega(R_t-R_e)^2/\hbar} \left|\frac{dV}{dR}\right|^{-1}_{R=R_t(E)}$$

where $R_t(E)$ is the classical turning point on the excited-state potential and μ is the reduced mass. The eigenvalue solutions for the X ^{1}A′ state were obtained using LEVEL 8.0[23] and fit to a truncated anharmonic oscillator to derive the harmonic frequency, ω = 924 cm^{-1}. The equilibrium distance, R_e = 1.33 Å, was taken from the X ^{1}A′ potential curve. The derivative of the excited-state potential, which was generated analytically after the ab initio data were fit to a multiorder polynomial, was evaluated over a range of energies. The resultant absorption spectrum as a function of excitation energy and corresponding wavelength is displayed in Figure 2 along with the ground-state probability amplitude, which was also generated using LEVEL 8.0.

The calculated UV absorption spectrum for CH_2OO peaks near 332 nm and falls off to half-maximum (363 nm) more steeply on the long-wavelength side; the absorption decreases more gradually (half-maximum at 255 nm) on the short-wavelength side. The calculated peak position and falloff to long wavelength (Figure 2) are in very good accord with the experimental spectrum (Figure 1). The asymmetric profile toward shorter wavelength will be examined in future work.

The UV spectrum of CH_2OO obtained in this work under jet-cooled conditions along with mass and isomer specificity through photoionization detection can be compared with prior reports in the literature. Both Sehested et al.[24] and Gravestock et al.[25] reported similar UV absorption spectra (peaked at ∼327 nm and spanning from 250 to 450 nm) following photolysis of CH_2I_2 and subsequent reaction with O_2 under flow-cell conditions, but these groups attributed the primary spectral carrier to be CH_2IOO. Taatjes and co-workers suggested that these prior reports may have included contributions from CH_2OO.[12] Lee et al.[18] computed vertical excitation energies for CH_2OO and CH_2IOO, which showed that the spectra of Sehested et al.[24] and Gravestock et al.[25] cannot be attributed completely to CH_2IOO. These earlier absorption spectra are substantially broader than the CH_2OO B ← X spectrum presented here (Figure 1), most likely because of absorption from other transient species including IO and CH_2I (primarily to shorter wavelength) and/or hot bands (toward longer wavelength).

We then utilized the absolute absorption cross section $\sigma(\lambda)$ across the B ← X spectrum to estimate the photochemical loss of CH_2OO upon solar irradiation. Using the maximum actinic flux $F(\lambda)$ at the Earth's surface (zenith angle of 0°),[1] which turns on near the peak of the CH_2OO absorption spectrum and increases markedly toward longer wavelength, the solar photolysis rate coefficient k_p can be calculated from the expression

$$k_p = \int_\lambda \varphi(\lambda)\sigma(\lambda)F(\lambda)\, d\lambda$$

The corresponding atmospheric lifetime $\tau = (k_p)^{-1}$ for CH_2OO is predicted to be on the order of 1 s, assuming that the photodissociation quantum yield $\varphi(\lambda)$ is unity. The same atmospheric lifetime was obtained using either the experimental or calculated absorption spectrum because the solar actinic flux limits the atmospherically relevant region to the long-wavelength side, where the experimental and calculated spectral contours are in excellent agreement.

The solar photolysis rate coefficient k_p for CH_2OO can be compared with its rate coefficients for bimolecular reactions with atmospheric pollutants under ambient air quality conditions. On the basis of the recently reported rate coefficients for the reactions of CH_2OO with SO_2 and NO_2[12] and average annual concentrations for these pollutants of 2 and 11 ppb, respectively,[26] the bimolecular loss of CH_2OO due to each of these reactions is expected to occur with a rate of ∼2 s^{-1}. The similarity of the estimated rates for bimolecular and photochemical loss processes suggests that solar photolysis may be a significant decay path for CH_2OO under daytime conditions in the troposphere. It is worth noting that direct dissociation of CH_2OO by solar irradiation yields O(^{1}D) photoproducts, which react with H_2O to produce secondary OH radicals.

In summary, we have reported a very strong UV absorption of the CH_2OO biradical due to the B ← X transition in the 320−350 nm region, providing a distinctive spectral signature of the Criegee intermediate for future laboratory and field studies. UV excitation was observed as a depletion of the ground-state population and corresponding VUV photoionization at 10.5 eV, providing mass- and isomer-specific detection of CH_2OO. UV excitation resulted in a large depletion (approaching 100%) due to direct dissociation as a result of the fully repulsive B-state potential along the O−O coordinate. The rate of photochemical loss of CH_2OO due to solar irradiation is predicted to be comparable to that for its key bimolecular reactions in the troposphere. Thus, UVA photolysis may play a significant role in the overall atmospheric lifetime of the Criegee intermediate in the daytime.

■ AUTHOR INFORMATION

Corresponding Author

milester@sas.upenn.edu

Notes

The authors declare no competing financial interest.

■ ACKNOWLEDGMENTS

This material is based on work supported by the National Science Foundation under Grant CHE-1112016. The authors thank C. A. Taatjes and J. M. Dyke for helpful discussions.

■ REFERENCES

(1) Finlayson-Pitts, B. J.; Pitts, J. N. *Chemistry of the Upper and Lower Atmosphere*; Academic Press: San Diego, 2000.

(2) Seinfeld, J. H.; Pandis, S. N. *Atmospheric Chemistry and Physics: From Air Pollution to Climate Change*, 2nd ed.; Wiley: New York, 2006.

(3) Wayne, R. P. *Chemistry of Atmospheres: An Introduction to the Chemistry of the Atmospheres of Earth, the Planets, and Their Satellites*, 3rd ed.; Oxford University Press: Oxford, U.K., 2000.

(4) Johnson, D.; Marston, G. *Chem. Soc. Rev.* **2008**, *37*, 699−716.

(5) Alam, M. S.; Camredon, M.; Rickard, A. R.; Carr, T.; Wyche, K. P.; Hornsby, K. E.; Monks, P. S.; Bloss, W. J. *Phys. Chem. Chem. Phys.* **2011**, *13*, 11002−11015.

(6) Donahue, N. M.; Drozd, G. T.; Epstein, S. A.; Presto, A. A.; Kroll, J. H. *Phys. Chem. Chem. Phys.* **2011**, *13*, 10848−10857.

(7) Criegee, R. *Angew. Chem., Int. Ed. Engl.* **1975**, *14*, 745−752.

(8) Horie, O.; Moortgat, G. K. *Acc. Chem. Res.* **1998**, *31*, 387−396.

(9) Calvert, J. G.; Atkinson, R.; Kerr, J. A.; Madronich, S.; Moortgat, G. K.; Wallington, T. J.; Yarwood, G. *The Mechanisms of Atmospheric Oxidation of the Alkenes*; Oxford University Press: Oxford, U.K., 2000.

(10) Mauldin, R. L., III; Berndt, T.; Sipila, M.; Paasonen, P.; Petaja, T.; Kim, S.; Kurten, T.; Stratmann, F.; Kerminen, V. M.; Kulmala, M. *Nature* **2012**, *488*, 193−196.
(11) Taatjes, C. A.; Meloni, G.; Selby, T. M.; Trevitt, A. J.; Osborn, D. L.; Percival, C. J.; Shallcross, D. E. *J. Am. Chem. Soc.* **2008**, *130*, 11883−11885.
(12) Welz, O.; Savee, J. D.; Osborn, D. L.; Vasu, S. S.; Percival, C. J.; Shallcross, D. E.; Taatjes, C. A. *Science* **2012**, *335*, 204−207.
(13) Huang, H.; Eskola, A. J.; Taatjes, C. A. *J. Phys. Chem. Lett.* **2012**, *3*, 3399−3403.
(14) Taatjes, C. A.; Welz, O.; Eskola, A. J.; Savee, J. D.; Osborn, D. L.; Lee, E. P. F.; Dyke, J. M.; Mok, D. W. K.; Shallcross, D. E.; Percival, C. J. *Phys. Chem. Chem. Phys.* **2012**, *14*, 10391−10400.
(15) Konen, I. M.; Pollack, I. B.; Li, E. X. J.; Lester, M. I.; Varner, M. E.; Stanton, J. F. *J. Chem. Phys.* **2005**, *122*, No. 094320.
(16) Werner, H.-J.; Knowles, P. J.; Manby, F. R.; Schütz, M.; Celani, P.; Knizia, G.; Korona, T.; Lindh, R.; Mitrushenkov, A.; Rauhut, G.; Adler, T. B.; Amos, R. D.; Bernhardsson, A.; Berning, A.; Cooper, D. L.; Deegan, M. J. O.; Dobbyn, A. J.; Eckert, F.; Goll, E.; Hampel, C.; Hesselmann, A.; Hetzer, G.; Hrenar, T.; Jansen, G.; Köppl, C.; Liu, Y.; Lloyd, A. W.; Mata, R. A.; May, A. J.; McNicholas, S. J.; Meyer, W.; Mura, M. E.; Nicklaß, A.; Palmieri, P.; Pflüger, K.; Pitzer, R.; Reiher, M.; Shiozaki, T.; Stoll, H.; Stone, A. J.; Tarroni, R.; Thorsteinsson, T.; Wang, M.; Wolf, A. *Molpro: A Package of ab Initio Programs for Molecular Electronic Structure Calculations*; University College Cardiff Consultants Limited: Cardiff, U.K.; 2010; version 2010.1; http://www.molpro.net/.
(17) Aplincourt, P.; Henon, E.; Bohr, F.; Ruiz-Lopez, M. F. *Chem. Phys.* **2002**, *285*, 221−231.
(18) Lee, E. P. F.; Mok, D. K. W.; Shallcross, D. E.; Percival, C. J.; Osborn, D. L.; Taatjes, C. A.; Dyke, J. M. *Chem.—Eur. J.* **2012**, *18*, 12411−12423.
(19) Matsumi, Y.; Kawasaki, M. *Chem. Rev.* **2003**, *103*, 4767−4781.
(20) Gutbrod, R.; Kraka, E.; Schindler, R. N.; Cremer, D. *J. Am. Chem. Soc.* **1997**, *119*, 7330−7342.
(21) Schinke, R. *Photodissociation Dynamics*; Cambridge University Press: Cambridge, U.K., 1993.
(22) Schinke, R.; Grebenshchikov, S. Y. *Phys. Chem. Chem. Phys.* **2007**, *9*, 4026−4029.
(23) Le Roy, R. J. *LEVEL 8.0: A Computer Program for Solving the Radial Schrodinger Equation*; University of Waterloo Chemical Physics Research Report CP-633; University of Waterloo: Waterloo, ON, 2007; http://scienide2.uwaterloo.ca/~rleroy/level/.
(24) Sehested, J.; Ellermann, T.; Nielsen, O. J. *Int. J. Chem. Kinet.* **1994**, *26*, 259−272.
(25) Gravestock, T. J.; Blitz, M. A.; Bloss, W. J.; Heard, D. E. *ChemPhysChem* **2010**, *11*, 3928−3941.
(26) U.S. Environmental Protection Agency. Air Quality Trends. http://www.epa.gov/airtrends/ (accessed Oct 22, 2012).